

Revisiting pseudo-Dirac neutrino scenario after recent solar neutrino data

Saeed Ansarifard* and Yasaman Farzan†

School of physics, Institute for Research in Fundamental Sciences (IPM)

P.O.Box 19395-5531, Tehran, Iran

(Dated: January 31, 2023)

It is still unknown whether the mass terms for neutrinos are of Majorana type or of Dirac type. An interesting possibility, known as pseudo-Dirac scheme combines these two with a dominant Dirac mass term and a subdominant Majorana one. As a result, the mass eigenstates come in pairs with a maximal mixing and a small splitting determined by the Majorana mass. This will affect the neutrino oscillation pattern for long baselines. We revisit this scenario employing recent solar neutrino data, including the seasonal variation of the ${}^7\text{Be}$ flux recently reported by BOREXINO. We constrain the splitting using these data and find that both the time integrated solar neutrino data and the seasonal variation independently point towards a new pseudo-Dirac solution with nonzero splitting for ν_2 of $\Delta m_2^2 \simeq 1.5 \times 10^{-11} \text{ eV}^2$. We propose alternative methods to test this new solution. In particular, we point out the importance of measuring the solar neutrino flux at the intermediate energies $1.5 \text{ MeV} < E_\nu < 3.5 \text{ MeV}$ (below the Super-Kamiokande detection threshold) as well as a more precise measurement of the pep flux. The code is available on Github

I. INTRODUCTION

Lepton flavor violation is the cornerstone of the modern neutrino physics, having been observed in various neutrino experiments such as solar, atmospheric, reactor and long baseline neutrino experiments. The three neutrino mass and mixing scheme has been established as the standard solution to the observed lepton flavor violation in evolution of neutrino states. It is not however known whether the neutrino mass term also violates lepton number or not. In other words, we do not know if the mass terms for neutrinos are of Majorana type or of Dirac type. In general, we can simultaneously write Majorana (μ) and Dirac mass (m) terms for neutrinos. At the limit where Majorana term is much smaller than the Dirac term (*i.e.*, in the limit $\mu \ll m$), the scheme is called pseudo-Dirac. This limit is of interest from both model building and phenomenological point of view. It is straightforward to show that the mass eigenstates composing the active states will split to pairs of Majorana states with maximal mixing and tiny mass squared differences given by $\Delta m^2 = \mu m$. For baselines much smaller than $E_\nu/(2\mu m)$, the neutrino oscillation pattern will be similar to what expected for the standard three neutrino mass and mixing scheme. For baselines comparable to $E_\nu/(2\mu m)$ or larger, the active to active neutrino oscillation probability will be smaller than that expected within the standard scheme as a part of the active flux can oscillate to sterile neutrinos. There is already rich literature on the potential of various neutrino observations to test this scenario. Upcoming terrestrial experiments such as DUNE and JUNO can test $\Delta m^2 \sim 10^{-5} \text{ eV}^2$ [1]. The galactic supernova neutrinos can probe Δm^2 down to 10^{-20} eV^2 [2]. Ultrahigh energy cosmic neutrinos can be sensitive to $\Delta m^2 > \text{few} \times 10^{-18} \text{ eV}^2$ [3–8]. Finally,

the solar neutrinos can be sensitive to $\Delta m^2 \gtrsim 10^{-13} \text{ eV}^2$ [9].

The possible effects of pseudo-Dirac neutrino scheme on solar neutrinos has been already discussed in the literature [9, 10]. Ref [9] constrains the splittings of ν_1 and ν_2 and finds a solution at $\sim 10^{-11} \text{ eV}^2$ for the neutrino data. Since the publication of Ref. [9], BOREXINO has released more data, with a relatively precise measurement of the pep flux as well as the measurement of seasonal flux variation. Moreover, the Super-Kamiokande data has been updated. We revisit the pseudo-Dirac scheme with the latest available BOREXINO and Super-Kamiokande solar data, also taking into account the precise measurement of Δm_{21}^2 by KamLAND. Similarly to Ref. [9], we find a solution with nonzero pseudo-Dirac splitting. We discuss the importance of the precise measurement of ${}^8\text{B}$ flux at energies between 1.5 MeV to 3 MeV (that is below the detection threshold of Super-Kamiokande and above the pep line) to test this solution.

In the range that the oscillation length due to the pseudo-Dirac mass splitting, Δm^2 , is comparable to the variation of the Earth-Sun distance during a year (resulting from the eccentricity of the Earth orbit), we expect a signature in the seasonal variation. We examine the recently reported seasonal variation of the ${}^7\text{Be}$ flux to search for such a variation. Independently of the time integrated analysis, this data also points towards a pseudo-Dirac solution with the same range of Δm^2 . We propose a few alternative methods to test this new non-trivial solution.

The paper is organized as follows: In sect. II, we review the oscillation of pseudo-Dirac neutrinos. This discussion is complemented in the appendix with a focus on matter effects as well as on the eccentricity of the Earth orbit. In sect. III, we summarize the basis of our analysis and define the relevant χ^2 tests. In sect. IV, we show the implications of the solar neutrino data for the pseudo-Dirac scheme. The concluding remarks and suggestions for further study are given in sect. V.

* ansarifard@ipm.ir

† yasaman@theory.ipm.ac.ir

II. OSCILLATION OF PSEUDO-DIRAC SOLAR NEUTRINOS

Within the pseudo-Dirac scheme, the neutrino states $\Psi^T = (\nu_L \ \nu_R)$ have both Dirac mass (m) and Majorana mass (μ) terms of form

$$\bar{\Psi}m\Psi + \bar{\Psi}^c\mu\Psi \quad \text{with } \mu \ll m \quad (1)$$

where $\Psi^c = -i\gamma^2\Psi^*$. In general, both m and μ are 3×3 matrices in the flavor space. For simplicity, we assume that m and μ can be simultaneously diagonalized. Then, as shown in the appendix, each Dirac mass eigenstate, ν_i splits to two Majorana states with a maximal mixing and a splitting of $\Delta m_i^2 = 2\mu_i m_i$. Thus, the ν_e survival probability and the probability of the conversion of ν_e into sterile neutrinos can be written as

$$P_{ee}(E_\nu, L, r) \equiv P(\nu_e \rightarrow \nu_e) = \quad (2)$$

$$\begin{aligned} & \cos^4 \theta_{13} \left(\cos^2 \theta_{12} \cos^2 \theta_M \cos^2 \left(\frac{\Delta m_1^2}{4E_\nu} L \right) \right. \\ & \quad \left. + \sin^2 \theta_{12} \sin^2 \theta_M \cos^2 \left(\frac{\Delta m_2^2}{4E_\nu} L \right) \right) \\ & + \sin^4 \theta_{13} \cos^2 \left(\frac{\Delta m_3^2}{4E_\nu} L \right) \end{aligned}$$

and

$$P_{es}(E_\nu, L, r) \equiv \sum_i P(\nu_e \rightarrow \nu_{si}) = \quad (3)$$

$$\begin{aligned} & \cos^2 \theta_{13} \left(\cos^2 \theta_M \sin^2 \left(\frac{\Delta m_1^2}{4E_\nu} L \right) \right. \\ & \quad \left. + \sin^2 \theta_M \sin^2 \left(\frac{\Delta m_2^2}{4E_\nu} L \right) \right) \\ & + \sin^2 \theta_{13} \sin^2 \left(\frac{\Delta m_3^2}{4E_\nu} L \right) \end{aligned}$$

where θ_M is the effective mixing at the production point of the ν_e inside the sun (at a distance of r from the Sun center) given by Eq. (A.10) in the appendix. L is the distance between Sun and Earth and E_ν is the neutrino energy.

The density profile of the Sun is exponentially suppressed with the distance from the Sun center so P_{ee} strongly depends on the production point, r . As explained in the appendix for each component of the solar flux component (*i.e.*, $j \in \{pp, {}^7\text{Be}, pep, {}^8\text{B}\}$) we should average $P_{ee}(E_\nu, L, r)$ and $P_{es}(E_\nu, L, r)$ over the production point, using the production point spatial distribution inside the Sun associated with each flux component. More details can be found in the appendix. Hereafter, we show the averaged survival probability over the production point of component j by $\bar{P}_{ee}^j(E_\nu, L)$. Fig. 1 illustrates the oscillation probability averaged with the distribution of ${}^8\text{B}$ production at several values of Δm_1^2

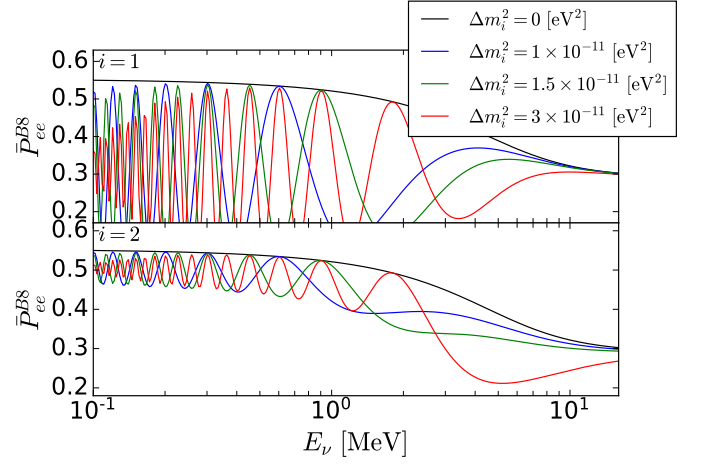


FIG. 1. Average survival probability of solar neutrinos, $P(\nu_e \rightarrow \nu_e)$ versus neutrino energy for various values of the splitting. Averaging is taken over the production point assuming the distribution of ${}^8\text{B}$ production. The L dependency is marginalized by taking temporal averaging on a year. (For more clarification see the bulk of the paper and the appendix.) The black curve corresponds to the pure standard MSW effect. The standard neutrino parameters are set equal to the best fit values as in [11]^a. In the upper (lower) panel, we have set $\Delta m_2^2 = 0$ ($\Delta m_1^2 = 0$) and only one Δm_i^2 is set nonzero. The blue, green and red lines respectively correspond to $\Delta m_i^2 = 1 \times 10^{-11} \text{ eV}^2$, $\Delta m_i^2 = 1.5 \times 10^{-11} \text{ eV}^2$ and $\Delta m_i^2 = 3 \times 10^{-11} \text{ eV}^2$.

^a NuFIT 5.1 (2021), www.nu-fit.org

and Δm_2^2 . The black lines correspond to the standard MSW solution. We expect for relatively large Δm_i^2 , the deviation to be more significant for large energies and relatively suppressed at low energies because the effect is given by the ratio $\Delta m_i^2/E_\nu$. This behavior is demonstrated by the red lines which correspond to Δm_1^2 or $\Delta m_2^2 = 3 \times 10^{-11} \text{ eV}^2$. For $\Delta m_i^2 \sim 10^{-11} \text{ eV}^2$, the deviation is specially significant for intermediate values of energies $1.5 \text{ MeV} < E_\nu < 3 \text{ MeV}$, lying below the detection threshold of Super-Kamiokande where the solar neutrino data is lacking.

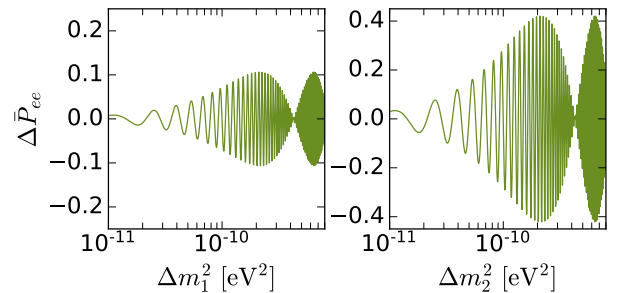


FIG. 2. $\Delta \bar{P}_{ee} = \bar{P}_{ee}^{Be7}(E_\nu, L_{max}) - \bar{P}_{ee}^{Be7}(E_\nu, L_{min})$ versus Δm_1^2 and Δm_2^2 at $E_\nu = 0.862 \text{ MeV}$ (*i.e.*, for ${}^7\text{Be}$ line). $L_{max} = 1.52 \times 10^8 \text{ km}$ and $L_{min} = 1.47 \times 10^8 \text{ km}$ are the Earth-Sun distance at aphelion and perihelion, respectively.

The average Sun Earth distance is ~ 150 million km but due to the eccentricity of the Earth orbit around the Sun, L varies during a year with $L_{max} - L_{min} = 5$ million km. Fig. 2 shows

$$\Delta \bar{P}_{ee} \equiv \bar{P}_{ee}^{7\text{Be}}(E_\nu, L_{max}) - \bar{P}_{ee}^{7\text{Be}}(E_\nu, L_{min})$$

versus Δm_1^2 and Δm_2^2 at $E_\nu = 0.862$ MeV which is the energy of the ^7Be line. As seen in these figures, for $\Delta m^2 > 10^{-11}$ eV 2 , the seasonal variation can be sizable. BOREXINO has recently published seasonal variation of the ^7Be flux reaching the Earth. We shall examine whether this piece of information can help to constrain the parameter space of the pseudo-Dirac scheme.

III. ANALYSIS OF THE SOLAR NEUTRINO DATA

As seen in Eqs. (2,3) and Eq. (A.10), the solar neutrino flux on the Earth depends on θ_{12} , Δm_{21}^2 and θ_{13} as well as on Δm_i^2 . Because of the smallness of $\sin^2 \theta_{13}$, the sensitivity of the solar data to θ_{13} is negligible so we fix $\theta_{31} = 8.57^\circ$ throughout our analysis [11]. Historically, the solar neutrino data have provided the first measurement of θ_{12} and Δm_{21}^2 within the standard neutrino mass and mixing paradigm (*i.e.*, setting $\Delta m_i^2 = 0$). These measurements were confirmed by the KamLAND reactor experiment which measured the $\bar{\nu}_e$ flux from reactors active throughout Japan. The baseline of KamLAND, L_{Kam} was less than 200 km so for the values of Δm_i^2 of our interest (10^{-12} eV $^2 \leq \Delta m_i^2 \leq 10^{-9}$ eV 2), we can write $\Delta m_i^2 L_{Kam} / (2E_\nu) \ll 1$. Thus, the neutrino oscillation in the KamLAND experiment was sensitive only to θ_{12} and Δm_{21}^2 . As a result, the determination of these parameters by KamLAND is also valid for our pseudo-Dirac scenario with $\Delta m_i^2 \neq 0 \ll 10^{-9}$ eV 2 . Indeed, the determination of Δm_{21}^2 by KamLAND suffers from much smaller uncertainty than that by the solar neutrino data. We therefore treat Δm_{21}^2 by a nuisance parameter with a mean value of $\bar{\Delta m}_{21}^2 = 7.54 \times 10^{-5}$ eV 2 and an error $\sigma_{\Delta m_{21}^2} = 0.5 \times 10^{-5}$ eV 2 as measured by KamLAND [12]. The effects of Δm_3^2 on P_{ee} and on P_{es} are respectively suppressed by $\sin^4 \theta_{13}$ and $\sin^2 \theta_{13}$ so the sensitivity to Δm_3^2 is low. We therefore set $\Delta m_3^2 = 0$ and focus on the effects of nonzero Δm_1^2 and Δm_2^2 on the solar neutrinos. We employ the latest solar data both from Super-Kamiokande and from BOREXINO to extract information on Δm_1^2 and Δm_2^2 . We also set θ_{12} as a free parameter to “re”-measured from the solar neutrino data in the presence of nonzero Δm_1^2 or Δm_2^2 .

We use the χ^2 analysis in order to constrain the allowed regions for the free parameters of the theory, separately defining χ^2 for each Δm_i^2 setting the rest equal to zero:

$$\chi_{\min}^2(\Delta m_i^2, \theta_{21}) = \quad (4)$$

$$\min_{\text{nuisance}} \left\{ \chi_{Su}^2 + \chi_{Bo}^2 + \left(\frac{\Delta m_{21}^2 - \bar{\Delta m}_{21}^2}{\sigma_{\Delta m_{21}^2}} \right)^2 \right\}$$

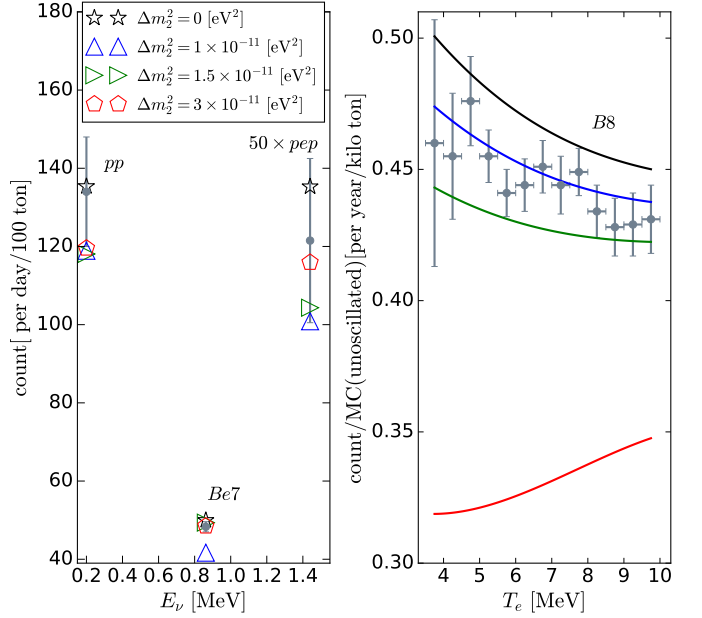


FIG. 3. The annually averaged BOREXINO (left) and Super-K (right) data points. Predictions for the splitting values of $\Delta m_2^2 = 1 \times 10^{-11}$ eV 2 (blue), $\Delta m_2^2 = 1.5 \times 10^{-11}$ eV 2 (green) and $\Delta m_2^2 = 3 \times 10^{-11}$ eV 2 (red) are illustrated. The standard MSW prediction (black) is added for comparison. We have taken $\Delta m_{21}^2 = 7.5 \times 10^{-5}$ eV 2 and $\theta_{12} = 33.4^\circ$ [11].

where Su (Bo) indicates the Super-Kamiokande (BOREXINO) experiment. χ_{Su}^2 is defined as follows [13]:

$$\chi_{Su}^2 = \sum_k \left[\left(\frac{D_k - f_k(\delta_B, \delta_S, \delta_R) \alpha^{B8} \mathcal{T}_k^{B8}}{\sigma_k} \right)^2 \right] + \left(\frac{\alpha^{B8} - 1}{\sigma_{\alpha^{B8}}} \right)^2 + \delta_B^2 + \delta_S^2 + \delta_R^2 \quad (5)$$

Subscript k runs over the 13 bins of ^8B solar neutrino energy spectrum starting from 3.5 MeV to 10 MeV. Super-Kamiokande covers the energy range 3.5 MeV to 19.5 MeV. However, the effect of Δm_i^2 in the range under study in this paper will be significant only at energies lower than 10 MeV. As a result, we do not consider the higher energy bins and we do not therefore need to worry about the *hep* data events. [14] Similarly for the BOREXINO experiment we have

$$\chi_{Bo}^2 = \sum_j \left[\left(\frac{D^j - \alpha^j \mathcal{T}^j}{\sigma^j} \right)^2 + \left(\frac{\alpha^j - 1}{\sigma_{\alpha^j}} \right)^2 \right] \quad (6)$$

Superscript j runs over pp , ^7Be and pep solar neutrino event rate (counts per day per 100 t).

D represent the background-subtracted measured data. σ include both statistical and systematic errors. Their values are taken from ref [15] and table 1 of ref [16] for Super-kamiokande and BOREXINO respectively. While the Super-Kamiokande data covers the solar neutrino spectrum with energies above 3.5 MeV, the

BOREXINO data provides precision measurement of the low energy part of the spectrum. The data used in Eqs. (5,6) is averaged over a year.

\mathcal{T} is the prediction which will be discussed below. α^j are added as nuisance parameters to account for the flux normalization uncertainty in the predictions of various solar neutrino components. The uncertainty values for pp and pep are taken equal to 1% and those for ${}^7\text{Be}$ and ${}^8\text{B}$ are taken equal to 6% and 12%, respectively [17]. We also consider the energy correlated systematic uncertainties in spectral shape, energy scale and energy resolution of ${}^8\text{B}$ by adding nuisance parameters δ_B, δ_S and δ_R , respectively. The dependence of $f_k(\delta_B, \delta_S, \delta_R)$ on the nuisance parameters and energy bins are explained in ref [18]. The prediction of the theory is derived by

$$\mathcal{T}_k^j(t_0, t_1, \Delta t) = \frac{t_0}{\Delta t} \mathcal{N}_{\text{det}} \int_{t_1}^{t_1 + \Delta t} dt \int dE_\nu \int_0^{T_e^{\text{max}}} dT_e \quad (7)$$

$$R_k^j(T_e) \phi^j(L) \frac{d\lambda^j}{dE_\nu}(E_\nu) \left[\frac{d\sigma_e}{dT_e}(E_\nu, T_e) \bar{P}_{ee}^j(E_\nu, L) + \frac{d\sigma_{\mu, \tau}}{dT_e}(E_\nu, T_e) \left(1 - \bar{P}_{ee}^j(E_\nu, L) - \bar{P}_{es}^j(E_\nu, L) \right) \right].$$

where Δt is the time period over which the temporal average is taken. For annually averaged data, Δt should be of course taken to be a year; then, \mathcal{T}_k^j will be independent of t_1 , i.e., independent of the start of the data taking period. t_0 determines the temporal unit of data which for the BOREXINO and Super-Kamiokande experiments are respectively taken to be a day and a year. For the BOREXINO experiment, $\mathcal{N}_{\text{det}} = 3.307 \times 31$ per 100 ton. For the Super-Kamiokande experiment, $\mathcal{N}_{\text{det}} = (10/18)(1/m_p)$ is the number of electron at each kilo ton of the Super-Kamiokande detector and m_p is the mass of the proton in kilotons. $R^j(T_e)$ is the detector performance function to measure the j th component. T_e is the recoil energy of the scattered electron. The $R^j(T_e) \sim 1$ for all three components ($pp, pep, {}^7\text{Be}$) because we have used the total event rate for the case of BOREXINO. $R_k^{B8}(T_e)$ for k th energy bin of ${}^8\text{B}$ follows a Gaussian function computed in Ref. [13].

$\phi^j(L)$ is the solar neutrino flux normalization:

$$\phi^j(L) \equiv \bar{\phi}^j \frac{\bar{L}^2}{L^2} \quad (8)$$

$\bar{\phi}^j$ is solar standard model prediction [17] calculated at \bar{L} , temporal average of sun to earth distance. L is the Sun to Earth distance which varies during a year due to the Earth orbit eccentricity. $\frac{d\lambda^j}{dE_\nu}(E_\nu)$ is the solar neutrino spectrum. For the pp and ${}^8\text{B}$ components which have continuous spectrum, $\phi^{pp}(L)(d\lambda^{pp}/dE_\nu)$ and $\phi^{B8}(L)(d\lambda^{B8}/dE_\nu)$ are in unit of $[\text{cm}^{-2}\text{s}^{-1}\text{MeV}^{-1}]$. The normalization of the monoenergetic ${}^7\text{Be}$ and pep fluxes are in the unit of $[\text{cm}^{-2}\text{s}^{-1}]$.

The differential cross sections of the electron scattered by neutrinos of different flavors (e, μ, τ) are [19]:

$$\frac{d\sigma_{e(\mu, \tau)}}{dT_e} = \frac{G_F^2 m_e}{2\pi} \left[\left(2 \sin^2(\theta_W) \pm 1 \right)^2 + \left(2 \sin^2(\theta_W) \left(1 - \frac{T_e}{E_\nu} \right) \right)^2 - 2 \sin^2(\theta_W) \left(2 \sin^2(\theta_W) \pm 1 \right) \frac{m_e T_e}{E_\nu^2} \right] \quad (9)$$

where for ν_e (for ν_μ, ν_τ) we should take the plus (minus) sign. We take the Weinberg angle as $\sin^2(\theta_W) = 0.22342$ [20]. The maximum recoil energy of the electron is given by

$$T_e^{\text{max}} = \frac{E_\nu^2}{E_\nu + m_e/2}.$$

IV. RESULTS

In sect. IV A, we first study how by combining the BOREXINO data on the ${}^7\text{Be}$, pep and pp event rate with the Super-Kamiokande solar neutrino spectrum data, we can constrain Δm_1^2 and Δm_2^2 . Surprisingly, we find that there is a new solution in the range of $\Delta m_2^2 = (1-2) \times 10^{-11} \text{ eV}^2$. We discuss whether the measurement of the total active neutrino fluxes by SNO or by current and future direct dark matter search experiments can test this new solution with nonzero Δm_2^2 . In sect. IV B, we study the effects of Δm_1^2 and Δm_2^2 on the seasonal variation of the ${}^7\text{Be}$ flux and contrast it with the recent BOREXINO data release on the seasonal variation of the ${}^7\text{Be}$ flux on the Earth. Surprisingly, this data independently points towards the same solution. We show that our new solution favors the GNO radio chemical experiment and is compatible with combined experiments Gallex and GNO [21]. We then discuss the prospect of testing this solution by a more precise measurement of the seasonal variation of the ${}^7\text{Be}$ flux.

A. Total solar flux integrated over year(s)

In this sub-section, we analyze the time-integrated BOREXINO and Super-Kamiokande solar neutrino data. The data points are shown in Fig. 3. The vertical axis in the left (right) panel is the number of counts per day per 100 tons (the number of counts over MC (unoscillated) per year per kilo ton). The prediction of the pseudo-Dirac scenario with $\Delta m_2^2 = (1, 1.5, 3) \times 10^{-11} \text{ eV}^2$ are also shown. To obtain these predictions, we have set $\Delta m_1^2 = 0$ and have used Eq. (7). The standard MSW scheme (i.e., $\Delta m_1^2 = \Delta m_2^2 = 0$) is added for comparison. As seen from the figure, large values of the splitting such as $\Delta m_2^2 \sim 3 \times 10^{-11} \text{ eV}^2$ can be ruled out by the ${}^8\text{B}$ data points. Although the range $\text{few} \times 10^{-12} \text{ eV}^2 < \Delta m_2^2 <$

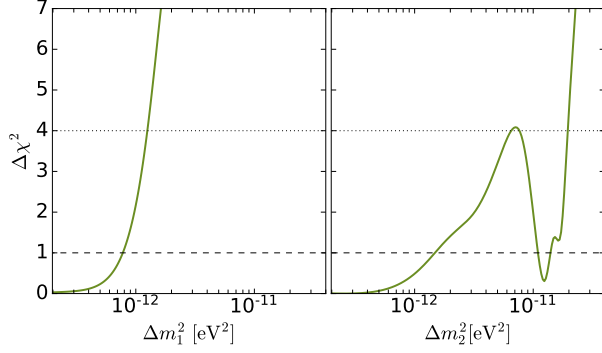


FIG. 4. $\Delta\chi^2$ as a function of Δm_i^2 minimized over θ_{12} . The dashed and dotted horizontal lines respectively correspond to the 68% and 95.45% confidence levels.

10^{-11} eV² is consistent with the Super-Kamiokande data, it is located out of one sigma error of the precise ⁷Be line measurement by BOREXINO. As demonstrated by the green curve and triangle, The $\Delta m_2^2 = 1.5 \times 10^{-11}$ eV² also gives a good fit to ⁸B data points as well as to the BOREXINO data points. Ref. [9] had also found this solution with $\Delta m_2^2 \sim 10^{-11}$ eV². Our results with updated solar data [16] which includes the relatively precise pep line measurement confirms their finding. Notice that the prediction with $\Delta m_2^2 = 1.5 \times 10^{-11}$ eV² for the pep line is smaller than that with $\Delta m_2^2 = 0$. Improving the precision of the pep line can therefore test this non-trivial solution.

Fig. 4 shows $\Delta\chi^2$ versus Δm_1^2 and Δm_2^2 . χ^2 is defined by Eq. (4). To compute $\Delta\chi^2$, we have minimized over θ_{12} and have subtracted the minimum χ^2 with respect to Δm_i^2 . As seen from the figure, the values of Δm_2^2 (Δm_1^2) larger than 2×10^{-11} eV² (1.5×10^{-12} eV²) is ruled out at 2σ . This figure also demonstrates that 1×10^{-11} eV² $< \Delta m_2^2 < 2 \times 10^{-11}$ eV² provides a fit comparable with SM when $\Delta m_2^2 \rightarrow 0$. [22] $\Delta m_2^2 < 1.5 \times 10^{-12}$ eV² is allowed within 1σ C.L. The 1σ and 2σ contours of Δm_2^2 versus θ_{12} are shown in Fig. 5. As seen from the figure, the values of θ_{12} at the solutions that we have found are consistent with the θ_{12} measurement by the global neutrino data analysis.

Let us now discuss the implication of the SNO measurement of the total active solar neutrino flux. The SNO experiment has extracted the total flux by measuring the Deuteron dissociation rate, $\nu + D \rightarrow \nu + n + p$ with a precision of 8% [23, 24]. This measurement is well-consistent with the standard solar model prediction for the total neutrino flux within the uncertainties. In our model, the measured total active flux is suppressed by $(1 - P_{es}(E_\nu))$. The SNO detection threshold is practically above 5 MeV. [25] For $E_\nu > 5$ MeV and $\Delta m_2^2 < 2 \times 10^{-11}$ eV², P_{es} is below 10% and as a result, the suppression of the total active flux measurement relative to the SM prediction will be within the flux prediction uncertainty of 12 % [17] and cannot therefore be resolved. For lower energies (below the SNO threshold), the deviation should

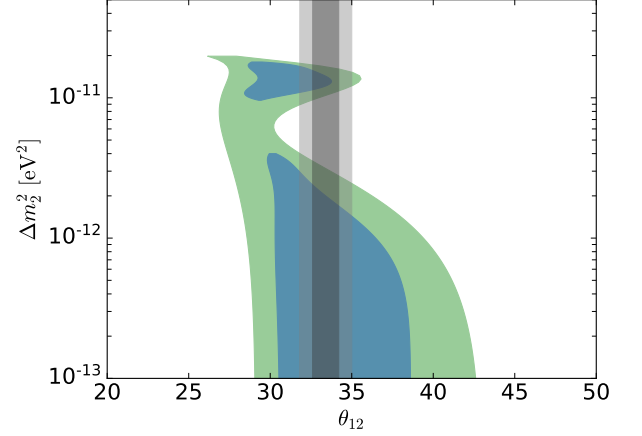


FIG. 5. Allowed 1σ and 2σ regions of joint χ^2 analysis for the $(\Delta m_2^2, \theta_{21})$ space, assuming Δm_1^2 is zero. The black and grey band show the 1σ and 2σ allowed range of θ_{12} by global neutrino data analysis [11].

be more significant. The total flux with lower energy threshold can also be measured by the coherent elastic neutrino nucleus scattering at large scale direct dark matter experiments such as the ongoing XENONnT and LZ experiments and future DARWIN experiment, promising to test this model.

B. Seasonal variation

Recently, the BOREXINO experiment has released data on the residual of the ⁷Be neutrino event rate, showing modulation due to the seasonal variation [26]. The selected events include an electron with a recoil energy larger than 0.3 MeV. The rate is given in terms of per day per 100t. The data points, covering a period of almost 10 years, are a time series binned in time intervals of 30 days. The annual trend of the data is subtracted. [27] We use this new data to independently examine the validity of the new solution ($\Delta m_2^2 \simeq (1 - 2) \times 10^{-11}$ eV²) found in sect. IV A. Furthermore, studying the seasonal variation is an alternative approach to probe the pseudo-Dirac mass splitting. The data points along with the predictions with various values of Δm_1^2 and Δm_2^2 are shown in Fig. 6.

As seen in Fig. 2, depending on the exact value of Δm_1^2 and/or Δm_2^2 in the range $\sim (1 - 2) \times 10^{-11}$ eV², the pseudo-Dirac scheme can lead to enhancement or suppression of the seasonal modulation. This behavior is also confirmed in Fig. 6. In the following, we focus on Δm_2^2 and set $\Delta m_1^2 = 0$. To constrain Δm_2^2 , we define χ^2 as

$$\chi^2 = \sum_t \frac{\left[D_t^{Be} - \left(\mathcal{T}^{Be}(\text{day}, t, m) - \mathcal{T}^{Be}(\text{day}, t, y) \right) \right]^2}{\sigma_t^2} \quad (10)$$

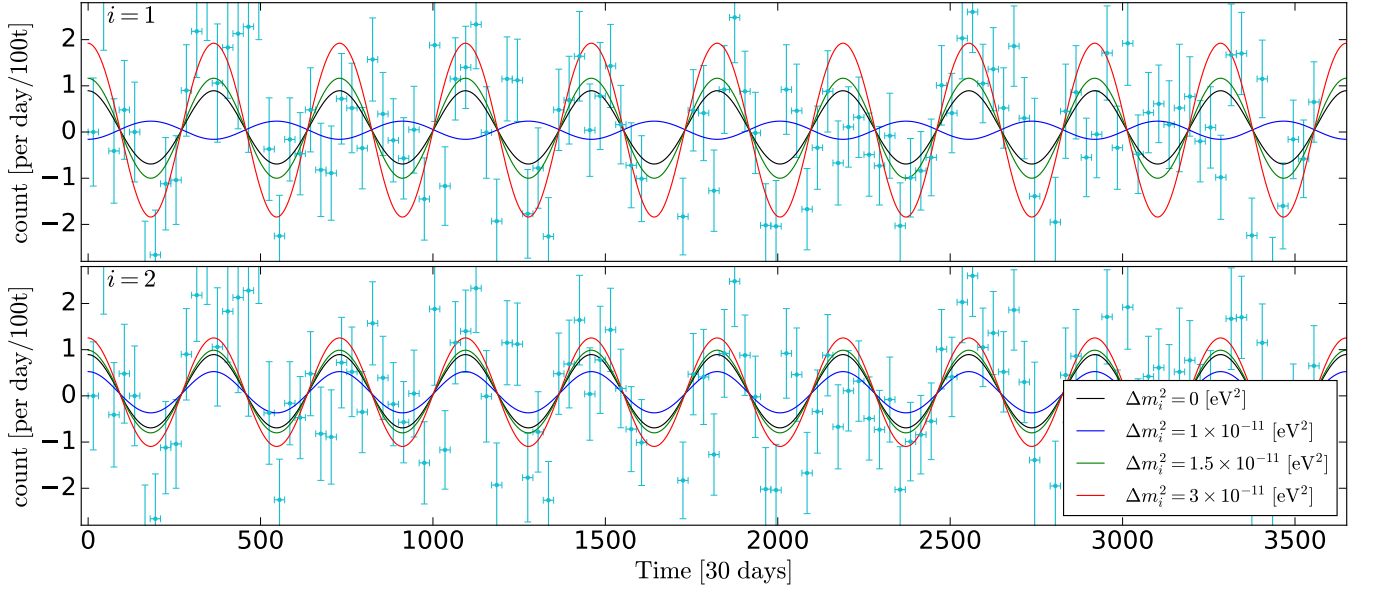


FIG. 6. Seasonal variation of event rate (per day per 100t) for ${}^7\text{Be}$. The data points are taken from [26]. The predictions for various values of Δm_i^2 are shown by curves. The upper (lower) panel corresponds to nonzero Δm_1^2 (nonzero Δm_2^2). The values of the standard mixing parameters are fixed to $\theta_{12} = 33.4^\circ$ and $\Delta m_{21}^2 = 7.5 \times 10^{-5} \text{ eV}^2$.

where t runs over the 120 bins, each bin corresponding to a one month data taking periods. m and y stand for month and year respectively. D_t^{Be} is residual of the events per day per 100 ton which are modeled as a time series trend [26]. σ_t^2 is the corresponding error at each bin t , as shown in Fig. 6. $\mathcal{T}^{Be}(\text{day}, t, \text{month})$ is computed using Eq. (7) by replacing the lower limit of the electron recoil energy with $T_e = 0.3 \text{ MeV}$ and integrating over monthly periods. $\mathcal{T}^{Be}(\text{day}, t, \text{year})$ is computed using the same formula with an averaging period of a year. As discussed before, $\mathcal{T}^{Be}(\text{day}, t, \text{year})$ should be independent of t . We fix $\theta_{12} = 33.4^\circ$, $\Delta m_{21}^2 = 7.54 \times 10^{-5} \text{ eV}^2$ and $\Delta m_1^2 = 0$ but vary Δm_2^2 . Similarly to the previous section, we invoke the standard solar model for the flux normalization, with negligible uncertainty. As seen from Fig. 7, the χ^2 analysis using this new data set independently supports the enhancement of the modulation which occur in the $1.4 \times 10^{-11} \text{ eV}^2 < \Delta m_2^2 < 2 \times 10^{-11} \text{ eV}^2$. This non-trivial solution falls in the 2σ region of the annually averaged data that we have found in sect. IV A. The non-trivial solution that we have found provides a better fit to the seasonal variation (see Fig. 7) than the standard model with $\Delta m_2^2 \rightarrow 0$. This is because the data shows about 10% more enhanced modulation than the $1/L^2$ modulation expected in the standard MSW scenario. On the other hand, a cancellation on the modulation takes place in the range $0.6 \times 10^{-11} \text{ eV}^2 < \Delta m_2^2 < 1.3 \times 10^{-11} \text{ eV}^2$ which is clearly ruled out with current data. The standard solution ($\Delta m_2^2 \rightarrow 0$) is allowed at just 80 % confidence level. However, the fact that the two independent measurements, namely the Super-Kamiokande time integrated solar data with $E_\nu > 3 \text{ MeV}$ and the seasonal varia-

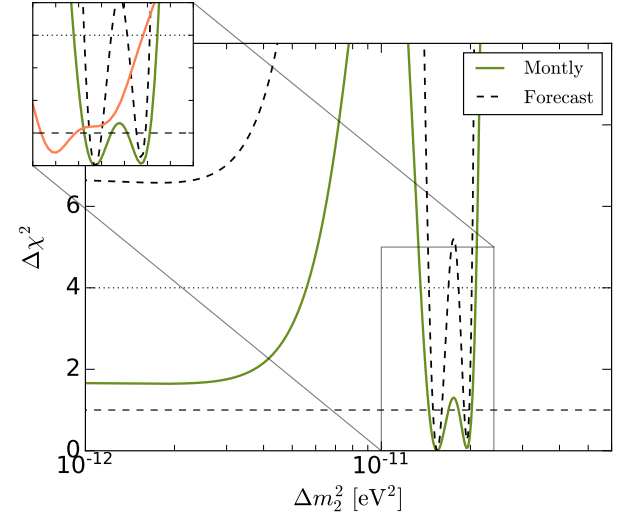


FIG. 7. $\Delta\chi^2$ as a function of Δm_2^2 using just the seasonal variation data set. The values of the standard mixing parameters are fixed to $\theta_{12} = 33.4^\circ$ and $\Delta m_{21}^2 = 7.54 \times 10^{-5} \text{ eV}^2$. The dashed curve illustrates the forecast for similar experiment with error $\sigma_t \sim 0.5$ per day per 100t; *i.e.*, with errors reduced to almost half of the current values. The right panel of Fig. 4 is added as orange curve for comparison in the zoomed box.

tion of the ${}^7\text{Be}$ flux measured by BOREXINO, as well as the time integrated BOREXINO solar neutrino data simultaneously point towards the same nonzero value of Δm_2^2 makes it imperative to look for ways to test this new solution.

We also examine this non-trivial solution with the data

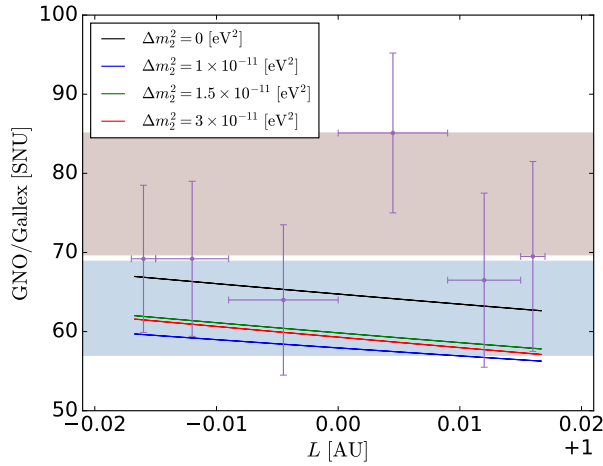


FIG. 8. Combined Gallex and GNO in solar neutrino unit (SNU) versus L . The color code for different Δm^2_2 is same as previous plots. The brown (blue) band is the 1σ allowed region derived by Gallex (GNO), averaging over time.

previously released by the radio chemical gallium experiments Gallex and GNO. We use the combined result for the variation of the total ν_e during a year. The data is taken from fig 7 of [21]. The results are illustrated in Fig. 8. These two experiments had capability to record the low energy ν_e above a threshold of 0.24 MeV. They might therefore be used to examine the low energy effect of pseudo-Dirac scheme for both annually averaged along with seasonal variation data. Although, the region of our interest, $\Delta m^2_2 \sim 1.5 \times 10^{-11} \text{eV}^2$, is compatible with the annually averaged data, due to large uncertainty the effect of seasonal variation is not apparent. The main source of uncertainties comes from the deviation of Gallex results from the GNO data. We have highlighted the 1σ averaged result of the Gallex in the Fig. 8 with light brown. It is clear that the combined result is affected by the tendency of Gallex data to higher values which is even at odds to the standard MSW scheme. We have also highlighted the 1σ averaged result of GNO with light blue. There is no preferences between the non-trivial solution and standard MSW when we just consider the GNO result at annually averaged level.

In the previous sections, we proposed four alternative methods to test this solution. In the following, we investigate how by improving the seasonal variation measurements, this new solution can be tested.

Let us suppose the true value of Δm^2_2 is close to the best fit that we have found and then study what level of precision is required to rule out the standard solution with $\Delta m^2_2 = 0$. The dashed line in Fig. 7 shows the value of $\Delta\chi^2$ versus Δm^2_2 setting $\sigma_t \sim 0.5$ (count/day per 100t). Notice that such σ_t requires a factor of 2 reduction in the current uncertainty. As seen from the figure, with such an improvement, the standard solution can be ruled out at better than 2σ C.L.

Let us now discuss how small σ_t should be in order

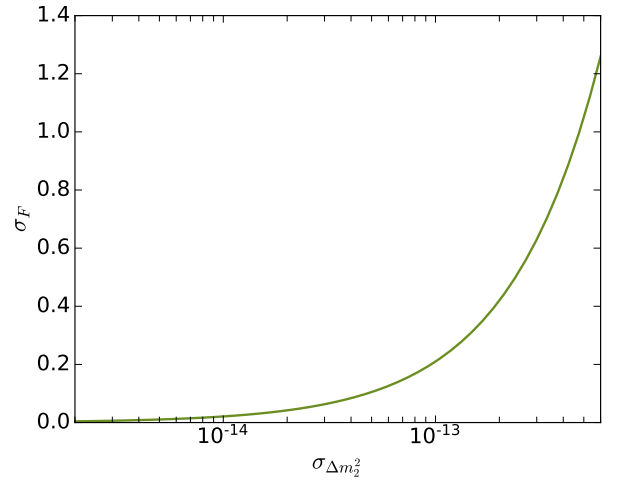


FIG. 9. The precision required in the time variation measurement to determine Δm^2_2 with a precision of $\sigma_{\Delta m^2_2}$. We have assumed that the true value is $\Delta m^2_2 = 1.5 \times 10^{-11} \text{eV}^2$.

to obtain a desired precision on Δm^2_2 . To answer this question, we assume that the error value $\sigma_t \sim \sigma_F$ is equal for all bins and utilize the Fisher forecast formalism [28] with

$$\sigma_F = \sigma_{\Delta m^2_i} \sqrt{\sum_t \left(\frac{\partial \mathcal{T}^{Be}(\text{day}, t, m)}{\partial \Delta m^2_i} \right)^2} \quad (11)$$

σ_F is the ideal measurement error in order to have $2 \times \sigma_{\Delta m^2_i}$, the 1σ allowed region for parameter Δm^2_i . The sum is over one year data points binned in 30 days and \mathcal{T}^{Be} is the prediction for ${}^7\text{Be}$ neutrino event rate with $T_e > 0.3$ MeV, similarly to the current measurement. We assume the true value $\Delta m^2_2 = 1.5 \times 10^{-11} \text{eV}^2$ which is in the range of $\sim (1-2) \times 10^{-11} \text{eV}^2$. The result is shown in Fig. 9. Error values of order of $\sigma_F \sim 1$ (count/day100t) lead to 1σ range $2 \times \sigma_{\Delta m^2_i} \sim 10^{-12} \text{eV}^2$. In particular, we obtain $2 \times \sigma_{\Delta m^2_i} \sim 0.5 \times 10^{-12} \text{eV}^2$ reducing them to $\sigma_F \sim 0.5$ (count/day100t).

V. DISCUSSION AND CONCLUSIONS

We have studied the oscillation of the solar neutrinos within the pseudo-Dirac scheme. Our focus has been on the splittings of ν_1 and ν_2 states, Δm^2_1 and Δm^2_2 of order of $10^{-13} \text{eV}^2 - 10^{-10} \text{eV}^2$ which are relevant for solar neutrinos. Since the contribution of ν_3 to the solar neutrinos (ν_e at the production) is suppressed by θ_{13} , a splitting in ν_3 will not affect the solar neutrino data. To derive bounds on the splitting, we have used the latest BOREXINO and Super-Kamiokande solar neutrino data and have employed the Δm^2_{21} measurement by KamLAND. We have found that these data rule out Δm^2_1 and Δm^2_2 above $2 \times 10^{-11} \text{eV}^2$. However, we find a new solution in the range of $\Delta m^2_2 \sim (1-2) \times 10^{-11} \text{eV}^2$ and $\Delta m^2_1 = 0$ which

fits the solar neutrino data (especially the ^8B data measured by Super-Kamiokande) in addition to the standard three neutrino scenario with $\Delta m_1^2 = \Delta m_2^2 = 0$. We have discussed the possibility of ruling out this solution with the total active neutrino flux measurement by SNO. We found that the deviation due to $P(\nu_e \rightarrow \nu_s)$ at this solution for neutrinos with energy above the SNO detection threshold can hide within the flux prediction. We have examined the robustness of this new solution against the accumulation of more solar data. The data available by 2016 slightly prefers this solution to the standard MSW. Ref. [9] also confirms this solution.

We have examined the possibility of testing this non-trivial pseudo-Dirac solution with the recent data release by BOREXINO on the seasonal variation of ^7Be [26]. Surprisingly, the seasonal variation also points towards a solution with $1.4 \times 10^{-11} \text{eV}^2 < \Delta m_2^2 < 2 \times 10^{-11} \text{eV}^2$, independently. Indeed, this solution fits the seasonal variation better than the standard three neutrino scheme but, the $\Delta m_1^2 = \Delta m_2^2 = 0$ solution is still allowed at 80% C.L. We have discussed how reducing the uncertainty in the measurement of seasonal variation can help to measure Δm_2^2 with better precision or set a bound on it.

We also examine our new solution with radio chemical gallium experiments Gallex and GNO. The solution is in agreement with the combined Gallex and GNO averaged results, favoring GNO over Gallex. However, due to large uncertainties it is not possible to test the effect of seasonal variation with this old data.

We have proposed four independent approaches to test the non-trivial solution that we have found: (1) Measurement of the ^8B flux in the energy range below 4 MeV with a moderate precision of 20 % (or better) can test

the solution. The proposed THEIA detector [29], with a relatively low detection energy threshold will be able to perform such a measurement. (2) By improving the precision of the measurement of the pep line, the solution can be tested. (3) Reducing the uncertainty in the seasonal variation of the ^7Be line by half can test this solution. (4) Finally, the measurement of the total active solar flux via coherent elastic ν nucleus scattering by direct dark matter search experiments can provide an alternative method for testing the solution.

We have found that both time integrated solar neutrino data and the ^7Be time variation, independently from each other, constrain $\Delta m_1^2 < 1.5 \times 10^{-12} \text{eV}^2$ and $\Delta m_2^2 < 2 \times 10^{-11} \text{eV}^2$ at 2σ C.L.

All material and code of this article are publicly available on <https://github.com/SaeedAnsarifard/SolarNeutrinos-pseudoDirac.git>

Appendix: Pseudo-Dirac scheme in the presence of matter

In this appendix, we derive dispersion relation and the energy momentum eigenstates for the pseudo-Dirac scheme in the presence of matter effects. We compute $P(\nu_e \rightarrow \nu_e)$ and $P(\nu_e \rightarrow \nu_s)$ for solar neutrinos in the pseudo-Dirac neutrino scheme. We then formulate the time dependence (seasonal variation) of the flux arriving to the Earth, considering the eccentricity of the Earth orbit around the Sun.

Let us start with one flavor state with the effective Lagrangian

$$\begin{aligned} \mathcal{L} &= \bar{\Psi} i \partial \cdot \gamma \Psi - m \bar{\Psi} \Psi - V \bar{\Psi} \gamma^0 P_L \Psi - \mu \bar{\Psi}^c P_R \Psi - \mu \bar{\Psi} P_L \Psi^c \\ &= \bar{\Psi}^c i \partial \cdot \gamma \Psi^c - m \bar{\Psi}^c \Psi^c + V \bar{\Psi}^c \gamma^0 P_R \Psi^c - \mu \bar{\Psi}^c P_R \Psi - \mu \bar{\Psi} P_L \Psi^c \end{aligned} \quad (\text{A.1})$$

where Ψ is a general Dirac spinor and $\Psi^c = -i\gamma^2 \Psi^*$. Taking the derivative of the Lagrangian in the first line of Eq. (A.1) with respect to $\bar{\Psi}$, we arrive at the Euler-Lagrange equation,

$$i \partial \cdot \gamma \Psi - m \Psi - V \gamma^0 P_L \Psi - \mu P_L \Psi^c = 0. \quad (\text{A.2})$$

Similarly taking derivative of the Lagrangian in the second line of Eq. (A.1) with respect to $\bar{\Psi}^c$, we find

$$i \partial \cdot \gamma \Psi^c - m \Psi^c + V \gamma^0 P_R \Psi^c - \mu P_R \Psi = 0. \quad (\text{A.3})$$

Applying $(i\gamma \cdot \partial - V\gamma^0 P_L)$ and $(i\gamma \cdot \partial + V\gamma^0 P_R)$ respectively to Eqs. (A.2, A.3), we obtain the following relations

$$\begin{aligned} -\partial^2 \Psi - 2iV P_L \partial_3 \Psi &= m^2 \Psi + m\mu \Psi^c - \mu^2 P_R \Psi \quad (\text{A.4}) \\ -\partial^2 \Psi^c + 2iV P_R \partial_3 \Psi^c &= m^2 \Psi^c + m\mu \Psi + \mu^2 P_L \Psi^c \end{aligned}$$

where we have taken the third (z) direction along the momentum (p) of the particle. Remembering $P_L \Psi = \nu_L$,

$P_L \Psi^c = \nu_R^c$, $P_R \Psi = \nu_R$, $P_R \Psi^c = -\nu_L^c$ and using $P_L P_R = 0$, we obtain

$$\begin{aligned} (E^2 - p^2) \begin{pmatrix} \nu_L \\ \nu_R^c \end{pmatrix} &= \begin{pmatrix} 2pV + m^2 & m\mu \\ m\mu & m^2 + \mu^2 \end{pmatrix} \begin{pmatrix} \nu_L \\ \nu_R^c \end{pmatrix} \quad (\text{A.5}) \\ &= \left[\begin{pmatrix} 2pV & 0 \\ 0 & 0 \end{pmatrix} + \begin{pmatrix} 0 & m \\ m & \mu \end{pmatrix}^2 \right] \begin{pmatrix} \nu_L \\ \nu_R^c \end{pmatrix} \end{aligned}$$

and

$$(E^2 - p^2) \begin{pmatrix} \nu_R \\ \nu_L^c \end{pmatrix} = \begin{pmatrix} m^2 - \mu^2 & -m\mu \\ -m\mu & m^2 - 2pV \end{pmatrix} \begin{pmatrix} \nu_R \\ \nu_L^c \end{pmatrix} \quad (\text{A.6})$$

Let us focus on Eq. (A.5). We should of course take the ultra relativistic limit, $p \gg V, m, \mu$ so the energy eigenvectors correspond to the eigenvectors of

$$\begin{pmatrix} V + \frac{m^2}{2p} & \frac{m\mu}{2p} \\ \frac{m\mu}{2p} & \frac{m^2 + \mu^2}{2p} \end{pmatrix}. \quad (\text{A.7})$$

In the limit $2Vp \ll m\mu$, we recover the famous pseudo-Dirac scheme with maximal mixing. That is the eigenstates will be the following Majorana states with energy eigenvalues as

$$\chi_1 = \frac{\nu_L + \nu_R^c}{2} \text{ with } E^2 = p^2 + m^2 + \mu m \quad (\text{A.8})$$

and

$$\chi_2 = \frac{\nu_L - \nu_R^c}{2} \text{ with } E^2 = p^2 + m^2 - \mu m \quad (\text{A.9})$$

As a result, active ν_L can oscillate to sterile neutrino with oscillation length determined by splitting $\Delta m^2 = 2m\mu$ and maximal mixing

$$P(\nu_L \rightarrow \nu_R^c) = \sin^2\left(\frac{\mu m}{2p}L\right)$$

and

$$P(\nu_L \rightarrow \nu_L) = 1 - P(\nu_L \rightarrow \nu_R^c) = \cos^2\left(\frac{\mu m}{2p}L\right)$$

Notice that the active and sterile neutrinos respectively correspond to ν_L and ν_R (or ν_R^c). We therefore use ν_R^c and ν_s interchangeably: $P(\nu_L \rightarrow \nu_R^c) = P(\nu_a \rightarrow \nu_s)$.

For $2pV \gg \mu m$, the mixing between ν_L and ν_R^c will be suppressed by $\mu m/(2pV)$ so the oscillation to sterile neutrino will be negligible. For the sake of simplicity, for the three neutrino flavors, we strict ourselves to the case that the m and μ matrices can simultaneously be diagonalized. Thus, in the mass basis all terms will be diagonal except for the effective potential $V \sum_{i,j} U_{ei} U_{ej}^* \bar{\Psi}_j \gamma^0 \Psi_i$.

Now, let us consider solar neutrinos with $\mu m/(2p) \sim 1/L$ where L is the Earth Sun distance. Within the Sun, the matter effects will dominate and will suppress the ν_{Li} and ν_{Ri}^c mixing. That is within the Sun, we shall have the standard MSW effect and the ν_e state after crossing the Sun will emerge at the Sun surface as an incoherent combination of ν_{L1} , ν_{L2} and ν_{L3} with pobabilities $\cos^2 \theta_M \cos^2 \theta_{13}$, $\sin^2 \theta_M \cos^2 \theta_{13}$ and $\sin^2 \theta_{13}$. Here, θ_M is the effective 12 mixing at the production point of ν_e :

$$\cos 2\theta_M = \quad (\text{A.10})$$

$$\frac{\Delta m_{21}^2 \cos 2\theta_{12} - V E_\nu}{[(\Delta m_{21}^2 \cos 2\theta_{12} - V E_\nu)^2 + (\Delta m_{21}^2 \sin 2\theta_{12})^2]^{1/2}}$$

in which $V = 2\sqrt{2}G_F N_e(r)|_{\text{at production}}$. Notice that we have taken into account two facts: (i) conversion in the Sun is adiabatic; (ii) the matter effect on θ_{13} is negligible due to suppression with $2Vp/(\Delta m_{31}^2 \sin \theta_{13}) \ll 1$. The mass eigenstates on their way to Earth can oscillate into their sterile counter-part (ν_{Ri}^c) with maximal mixing so the survival probability up to the Earth surface can be

written as

$$P_{ee} = \cos^4 \theta_{13} \left(\cos^2 \theta_{12} \cos^2 \theta_M \cos^2 \left(\frac{\mu_1 m_1}{2p} L \right) + \sin^2 \theta_{12} \sin^2 \theta_M \cos^2 \left(\frac{\mu_2 m_2}{2p} L \right) + \sin^4 \theta_{13} \cos^2 \left(\frac{\mu_3 m_3}{2p} L \right) \right) \quad (\text{A.11})$$

and

$$P_{es} = \cos^2 \theta_{13} \left(\cos^2 \theta_M \sin^2 \left(\frac{\mu_1 m_1}{2p} L \right) + \sin^2 \theta_M \sin^2 \left(\frac{\mu_2 m_2}{2p} L \right) + \sin^2 \theta_{13} \sin^2 \left(\frac{\mu_3 m_3}{2p} L \right) \right) \quad (\text{A.12})$$

For simplicity, we denote $P_{ee} \equiv P(\nu_e \rightarrow \nu_e)$ and $P_{es} \equiv \sum_i P(\nu_e \rightarrow \nu_{si})$. This formula corresponds to that in Ref. [10] in the limit $\mu_i m_i \ll V E_\nu$. For relatively high energy solar neutrinos, the oscillation in Earth due to matter effects (*i.e.*, Day/Night effect) can also be important but our focus is on the intermediate energy solar neutrinos for which the matter effects are negligible.

Through θ_M , P_{ee} depends on the location of ν_e production inside the Sun. We define

$$\bar{P}_{ee}^j(E_\nu, L) = \int_0^{R_\odot} P_{ee}(E_\nu, L, r) \Phi_j(r) dr \quad (\text{A.13})$$

where j can be any of the flux components pp , ${}^7\text{Be}$, pep and ${}^8\text{B}$. $\Phi_j(r)$ is the flux from radius r taken from [30]. Notice that $\Phi_j(r)dr$ includes the volume factor ($r^2 dr$) in its definition and vanishes at $r = 0$. The dependence of $\Phi_j(r)$ on r is different for the j modes. For example, while for $j = pp$ the flux peaks at $r \simeq 0.1R_\odot$, for $j = {}^8\text{B}$, the peak is at $r \simeq 0.05R_\odot$. The dependence of $P_{ee}(E_\nu, L, r)$ on r is through the dependence of θ_M on $N_e(r)$. Let us define

$$\Delta m_i^2 = 2\mu_i m_i.$$

Let us now discuss the time dependence of the flux throughout a year. The sun Earth distance during a year varies between $L_{max} = 152.1 \times 10^6$ km (aphelion occurring around July 4th) and $L_{min} = 147.1 \times 10^6$ km (perihelion occurring around January 4th). That is the orbit of the Earth around the Sun can be written as

$$L(\theta) = \frac{a(1 - e^2)}{1 + e \cos \theta} \quad (\text{A.14})$$

in which $a = (L_{min} + L_{max})/2$ and the eccentricity is $e = (L_{max} - L_{min})/(L_{max} + L_{min}) = 0.0167$. The conservation of the angular momentum implies $dt = (L^2/H)d\theta$

in which $H = |\vec{r} \times \dot{\vec{r}}|$. The number of events during a time interval (T_1, T_2) is proportional to

$$\int_{t_1}^{t_1+\Delta t} \frac{P_{ee}\sigma_e + (1 - P_{ee} - P_{es})\sigma_\mu}{L^2} dt = \quad (\text{A.15})$$

$$\int_{\theta_1}^{\theta_2} \frac{P_{ee}\sigma_e + (1 - P_{ee} - P_{es})\sigma_\mu}{H} d\theta$$

where σ_e and σ_μ are respectively the scattering cross sections of ν_e and ν_μ (or ν_τ) at the detector. To compute the number of events during a time interval we should know the relation between θ and time. Replacing $L(\theta)$ given in Eq. (A.14) we find

$$\int_{t_1}^{t_1+\Delta t} \frac{H}{a^2(1-e^2)^2} dt = \int_{\theta_1}^{\theta_2} \frac{d\theta}{(1+e\cos\theta)^2} \quad (\text{A.16})$$

which yields

$$H = \frac{6.55a^2(1-e^2)^2}{1 \text{ year}}.$$

We have used these formulas to study the seasonal variation of the ${}^7\text{Be}$ solar flux. As shown in [31], the

widths of ${}^7\text{Be}$ and pep lines are of order of kinetic energy in the sun center $\Delta E_\nu \sim 0.6$ keV. Thus, as long as $\Delta m^2 L/E \ll 1000$, we have $(\Delta E_\nu/E_\nu)(\Delta m^2 L/E) \ll 1$, the finite width of these lines will not smear the oscillatory behavior.

ACKNOWLEDGMENTS

The authors are grateful to P. Zakeri for the collaboration in the early stages of this work. This project has received funding/support from the European Union's Horizon 2020 research and innovation programme under the Marie Skłodowska-Curie grant agreement No 860881-HIDDeN. YF has received financial support from Saradaman under contract No. ISEF/M/401439. She would like to acknowledge support from the ICTP through the Associates Programme and from the Simons Foundation through grant number 284558FY19.

-
- [1] G. Anamiati, V. De Romeri, M. Hirsch, C. A. Ternes, and M. Tórtola, Phys. Rev. D **100**, 035032 (2019), arXiv:1907.00980 [hep-ph].
- [2] I. Martinez-Soler, Y. F. Perez-Gonzalez, and M. Sen, Phys. Rev. D **105**, 095019 (2022), arXiv:2105.12736 [hep-ph].
- [3] A. Esmaili and Y. Farzan, JCAP **12**, 014, arXiv:1208.6012 [hep-ph].
- [4] A. S. Joshipura, S. Mohanty, and S. Pakvasa, Phys. Rev. D **89**, 033003 (2014), arXiv:1307.5712 [hep-ph].
- [5] R. M. Crocker, F. Melia, and R. R. Volkas, Astrophys. J. Suppl. **130**, 339 (2000), arXiv:astro-ph/9911292.
- [6] A. Esmaili, Phys. Rev. D **81**, 013006 (2010), arXiv:0909.5410 [hep-ph].
- [7] P. Keranen, J. Maalampi, M. Myrskylainen, and J. Riittinen, Phys. Lett. B **574**, 162 (2003), arXiv:hep-ph/0307041.
- [8] R. M. Crocker, F. Melia, and R. R. Volkas, Astrophys. J. Suppl. **141**, 147 (2002), arXiv:astro-ph/0106090.
- [9] G. Anamiati, R. M. Fonseca, and M. Hirsch, Phys. Rev. D **97**, 095008 (2018), arXiv:1710.06249 [hep-ph].
- [10] A. de Gouvea, W.-C. Huang, and J. Jenkins, Phys. Rev. D **80**, 073007 (2009), arXiv:0906.1611 [hep-ph].
- [11] I. Esteban, M. C. Gonzalez-Garcia, M. Maltoni, T. Schwetz, and A. Zhou, JHEP **09**, 178, arXiv:2007.14792 [hep-ph].
- [12] A. Gando *et al.* (KamLAND), Phys. Rev. D **83**, 052002 (2011), arXiv:1009.4771 [hep-ex].
- [13] K. Abe *et al.* (Super-Kamiokande), Phys. Rev. D **94**, 052010 (2016), arXiv:1606.07538 [hep-ex].
- [14] Regarding to day/night effect see the Appendix.
- [15] Y. Nakajima (Super-Kamiokande), Talk given at the XXIX International Conference on Neutrino Physics and Astrophysics, June 30 (2020).
- [16] M. Agostini *et al.* (BOREXINO), Eur. Phys. J. C **80**, 1091 (2020), arXiv:2005.12829 [hep-ex].
- [17] N. Vinyoles, A. M. Serenelli, F. L. Villante, S. Basu, J. Bergström, M. C. Gonzalez-Garcia, M. Maltoni, C. Peña Garay, and N. Song, Astrophys. J. **835**, 202 (2017), arXiv:1611.09867 [astro-ph.SR].
- [18] Y. Nakano (Super-Kamiokande), PhD thesis, Tokyo U. (2016).
- [19] Z. Chen, T. Li, and J. Liao, JHEP **05**, 131, arXiv:2102.09784 [hep-ph].
- [20] <https://pdg.lbl.gov/>.
- [21] M. Altmann *et al.* (GNO), Phys. Lett. B **616**, 174 (2005), arXiv:hep-ex/0504037.
- [22] We have also performed a similar analysis with the official Super-Kamiokande data release in 2016 [13] which confirmed the current results, except that those data tended to have lower values and thus the region found in the interval of $\Delta m_2^2 = (1, 2) \times 10^{-11}$ compared to the $\Delta m_2^2 \rightarrow 0$ have lower χ^2 value; *i.e.*, providing a slightly better fit than the standard MSW with $\Delta m_2^2 = 0$.
- [23] B. Aharmim *et al.* (SNO), Phys. Rev. C **88**, 025501 (2013), arXiv:1109.0763 [nucl-ex].
- [24] B. Aharmim *et al.* (SNO), Phys. Rev. C **87**, 015502 (2013), arXiv:1107.2901 [nucl-ex].
- [25] The natural energy threshold, which is set by the binding energy of the Deuteron nucleus, is 2.2 MeV.
- [26] S. Appel *et al.* (BOREXINO), Astropart. Phys. **145**, 102778 (2023), arXiv:2204.07029 [hep-ex].
- [27] For the exact definition of tend and residue, the readers may consult [26].
- [28] M. Tegmark, A. Taylor, and A. Heavens, Astrophys. J. **480**, 22 (1997), arXiv:astro-ph/9603021.

- [29] M. Askins *et al.* (Theia), Eur. Phys. J. C **80**, 416 (2020), arXiv:1911.03501 [physics.ins-det].
- [30] [Http://www.sns.ias.edu/~jnb/](http://www.sns.ias.edu/~jnb/).
- [31] J. N. Bahcall, Phys. Rev. D **49**, 3923 (1994), arXiv:astro-ph/9401024.